

Impact of Vehicle Type and Headlight Characteristics on Vehicular VLC Performance

Agon Memedi*, Claas Tebruegge^{†*}, Julien Jahneke* and Falko Dressler*

*Heinz Nixdorf Institute and Dept. of Computer Science, Paderborn University, Germany

[†]HELLA GmbH & Co. KGaA, Lippstadt, Germany

{memedi, julien.jahneke, dressler}@ccs-labs.org, claas.tebruegge@hella.com

Abstract—We investigate the impact of various headlight modules and corresponding vehicle types on the performance of Vehicular VLC (V-VLC). V-VLC is currently considered as a quite promising communication technology that is complementary to existing wireless radio-based systems. Being a line of sight communication system, V-VLC is suggested mainly for shorter range communication causing little interference to concurrently performed transmissions. Given the very promising results in the literature, we study the impact of realistic headlight modules and vehicle types. Based on photometric data and experimental validation, we show that there is a substantial impact on the communication performance. The different light distribution patterns result in a varying light density and, therefore, packet delivery ratio. We see our models as an important step towards turning V-VLC into a reliable communication technology.

I. INTRODUCTION

Traffic accidents involving vehicles remain one of the leading causes of fatalities worldwide, although these numbers have reduced in the period between 2006–2014 [1]. The reduction in fatalities can be partially attributed to the technological advancements in safety systems in modern vehicles. However, in order to further reduce the number of fatalities on roads one can take advantage of Intelligent Transportation Systems (ITS). Among others, ITS suggest the integration of communication capabilities into road infrastructure and vehicles in order to enable Inter-Vehicle Communication (IVC) communications [2]. Typically, RF-based communication technologies like Dedicated Short Range Communication (DSRC) and LTE-based Cellular V2X (C-V2X) have been utilized for such applications. However, despite years of research and development, there are still doubts regarding their ability to satisfy the stringent reliability and latency requirements of safety-critical ITS applications, particularly when considering network outages or malicious security incidents [3]. As a result, the research community is considering novel, complementary communication technologies for IVC.

Driven by the rapid adoption of Light Emitting Diodes (LEDs) as main luminaries in exterior automotive lighting (i.e., headlights and taillights), Visible Light Communication (VLC) has emerged as a viable access technology for vehicular networking [4]–[6]. Data communication in Vehicular VLC (V-VLC) is realized by exploiting the fast switching capability of LEDs deployed in vehicles' exterior lighting modules. Information is modulated onto the intensity of the LEDs at speeds undetectable to the human eye, and it is received

by photosensitive devices (e.g., Photodiode (PD) or camera image sensors), which recover the original information from the generated photocurrent. Since V-VLC operates in the visible light portion of the electromagnetic spectrum, it can be used alongside RF-based communications as a complementary technology. For instance, the short range and directional nature of VLC results in a smaller collision domain compared to that of RF communications. In turn, this results in less packet loss caused from interference. The directionality also has implications in terms of security, as it is highly unlikely that an eavesdropper trying to intercept the VLC link remains unnoticed, as VLC typically requires Line Of Sight (LOS).

Historically, exterior lighting modules in vehicles serve for safety purposes by providing adequate road illumination and signaling. Since the emitted light is perceivable to the human eye, there exist standards that regulate certain aspects of the emitted light, such as the average optical power [7] or the shape of the radiation pattern [8]. These standards, however, do not impose strict constraints on the aesthetical and technical design of the lighting modules. As a result, there is huge variety in lighting modules depending on vehicle type, model, manufacturer, etc. Moreover, by design, exterior lighting modules consist of multiple sub-modules, (e.g., a modern headlight comprises of a Daytime Running Light (DRL), fog light, low beam, high beam), each of which have different light radiation characteristics. In theory, different vehicle types with different sub-modules can all communicate via V-VLC. However, the differences in lighting module design are non-negligible and they can affect the quality of the V-VLC.

In this paper, we investigate the performance impact of different headlights (low beam and high beam) of different vehicles on V-VLC. The radiation patterns of the used lighting modules are based on photometric data from HELLA GmbH & Co. KGaA, which we integrate to the well-known Veins vehicular network simulation framework [9] and make publicly available as Open Source¹. Based on an extensive simulation study, we are able to show that this impact is indeed non-negligible and must be inherently considered when designing V-VLC communication systems and applications. Our findings also reveal that not only the lighting module has a significant impact but particularly also the vehicle type. We see the presented results as a first step towards a handbook for vehicle

¹<http://ccs-labs.org/software/veins-vlc/>

and lighting module manufacturers for design guidelines needed to successfully integrate V-VLC for many safety applications.

Our main contributions can be summarized as follows:

- We introduce a modeling approach for V-VLC using different vehicle types and lighting modules.
- We exemplarily model a set of lighting modules based on a library of photometric data and also experimentally validate these data in a specially designed measurement facility.
- We integrate the resulting models into the Open Source simulation framework Veins to investigate the impact not only on photometric measures but also on V-VLC communication metrics.

II. RELATED WORK

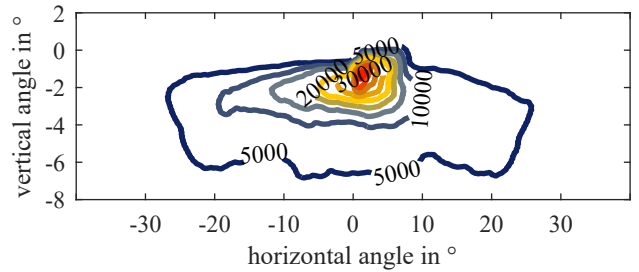
With the growing popularity of V-VLC in recent years, a large number of studies in the literature have addressed different aspects of this technology. Experimental studies in this domain mostly focus on physical layer aspects, such as the feasibility of lighting modules for VLC [4], [10], hardware prototyping of V-VLC systems [11], and the design and implementation of efficient and robust modulation schemes [12].

For instance, Narmanlioglu et al. [12] perform empirical measurements to investigate the feasibility of using multiple OFDM modulated taillights and multiple PDs for LOS and beyond LOS Vehicular VLC communication. In another experimental study, Turan et al. [13] use the fog lights of a real vehicle to realize V-VLC. The fog lights on each side of the vehicle are used to transmit the same data, showing that dual channel communication improves the Packet Delivery Ratio (PDR) at short distances. Tseng et al. [10] perform measurements for a vehicle's left headlight and taillight and report about the asymmetry in radiation characteristics between the two lighting modules.

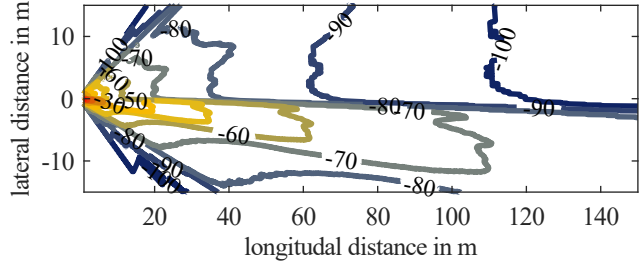
All of the aforementioned works are based on the investigation of the exterior lighting modules of one vehicle; this may limit the conclusions drawn from those studies to the particular vehicle type. However, vehicles (and exterior lighting modules) come with different design characteristics, which may impact their radiation properties and V-VLC performance. For instance, for the case of IEEE 802.11p-based vehicular communication, Eckhoff et al. [14] showed that radiation patterns of different antenna designs affect the network topology and have crucial impact on safety applications.

Simulation is the main methodology to study vehicular networks at larger scale and enable us to investigate the effect of variations in vehicle properties and design. However, the outcome of such studies relies upon the quality of the used models. Tomas et al. [15] present a V-VLC transceiver module for the JiST/SWANS simulator. The proposed module uses a simplified path loss model and is not able to simulate node mobility.

Viriyasitavat et al. [16] show that the generalized Lambertian model, which is typically used for LED luminaries, cannot accurately estimate the received power transmitted from a scooter's LED-based taillight. As a solution, the authors



(a) Isocandela curves showing angular distribution of luminous intensity



(b) Spatial distribution of signal strength P_{PD} in dBm with 0dB gain and no height difference between Tx and Rx

Figure 1. Goniometric measurements used as input data, and the estimated spatial distribution of the power at PD's output.

propose a model with fitted parameter values specified based on a threshold irradiance angle.

Luo et al. [17] present an analytical V-VLC model, which accounts both for the LOS and the Non Line Of Sight (NLOS) link reflected from the road. Also, the reflection characteristics of different road surface materials under different weather conditions are considered. The authors compare the radiation characteristics of low beams and high beams from a market-weighted database of measured tungsten halogen headlights, and investigate the BER performance of low beams under different dirt conditions. The results show that the NLOS reflection is stronger in wet road conditions, and a low-mounted PD has positive impact on the BER performance of the low beam for greater communication distances. This study, however, lacks thorough empirical validation.

In our previous work [18], we introduced a simulation model for V-VLC based on simple real-world empirical measurements. In this work, we go one step further and study the impact of headlight radiation patterns for V-VLC using a new model which for the first time takes into consideration specific vehicle types and light modules.

III. MODELING V-VLC SIGNAL DISTRIBUTION

A. Line-of-Sight Simulation Model

A combination of measurements and analytical calculations are required to realistically model the spatial signal distribution of lighting modules for our simulations. First, we obtain the photometric data of various lighting modules of road-licensed cars either measured with a specially designed optical goniometer (i.e., goniophotometer) with high angular resolution or generated via accurate optical simulations. These measurements provide the light distribution as luminous intensity for a range

of horizontal and vertical angles $I_V(\alpha_h, \alpha_v)$. Figure 1a shows the measured luminous intensity of the left low beam of a sedan car. In photometry, the power emitted by a light source is weighted by the sensitivity of the human eye $V(\lambda)$; hence we need to transform the luminous intensity to radiometric units which can be used to investigate the spatial distribution of the signal strength for V-VLC.

In the following, we perform the required transformations in a step by step fashion; this way, we gradually get from a general representation of the received signal to a hardware-specific one; our model assumes a PD is deployed on the receiving side. Using geometrical information of the scenario between the transmitter and the receiver (i.e., distance r , horizontal angle α_h , and vertical angle α_v), and considering the effective area of the PD $A_{PD,eff}$, from the luminous intensity $I_V(\alpha_h, \alpha_v)$ we can calculate the light received at a PD as luminous flux $\Phi_{V,\Omega}$ [19]

$$\Phi_{V,\Omega} = \iint_{\Omega} I_V(\alpha_h, \alpha_v) d\Omega, \quad (1)$$

where Ω is the solid angle projected on the area of the PD, given as [20]

$$\Omega = \frac{A_{PD,eff}}{r^2}. \quad (2)$$

In general, if we assume that the receiver is a surface A_{PD} tilted by angle θ , the effective area of the PD $A_{PD,eff}$ can be calculated by

$$A_{PD,eff} = A_{PD} \cdot \cos(\theta). \quad (3)$$

With appropriate adjustments to the formula, we could also consider any optic elements in front of the PD; for simplicity, here we consider a plain surface for the receiver with no optic elements in front.

In the next step, we perform the power conversion from luminous flux to the electrical current at the PD I_{PD} , by considering the spectrum of the LED and the PD. Since the luminous flux $\Phi_{V,\Omega}$ is a photometric quantity, first it has to be converted to the radiometric radiant flux $\Phi_{E,\Omega}$

$$\Phi_{E,\Omega} = \int_0^{\infty} \frac{d\Phi_{V,\Omega}(\lambda)}{K_m \cdot V(\lambda)} d\lambda = K^{-1} \cdot \Phi_{V,\Omega}, \quad (4)$$

where K_m is the maximum value of the photometric radiation equivalent, $V(\lambda)$ is the luminosity function which represents the sensitivity of the human eye, and K is the photometric radiation equivalent for a specific LED spectrum. Here, we can calculate the integral only once for a specific LED and afterwards use the K^{-1} constant to perform the conversion from photometric to radiometric quantities.

$\Phi_{E,\Omega}$ gives us a generic observation (without a spectral weighting) of how much radiation is collected at a specific area. For an even more generic observation, one can calculate the irradiance E_e , which gives the density of the radiation independent of the receiver surface.

Next, to account for specific hardware, we need to consider the parameters of the PD when calculating the photocurrent I_{PD} . The most important parameters are the size of the PD

and the responsivity curve \mathcal{R} , which describes the wavelength-dependent current output of the PD. We calculate the photocurrent I_{PD} by considering the spectrum of the PD and the spectrum of the LED

$$I_{PD} = \int_0^{\infty} \frac{d\Phi_{V,\Omega}(\lambda) \cdot \mathcal{R}(\lambda)}{K_m \cdot V(\lambda)} d\lambda = K_{PD}^{-1} \cdot \Phi_{V,\Omega}, \quad (5)$$

where K_{PD}^{-1} is the constant to calculate the photocurrent from the luminous flux on the receiver surface for a specific LED and PD combination. Usually, the next step in the transmission chain is the current-to-voltage conversion and amplification with a Transimpedance Amplifier (TIA). This can be calculated by converting the photocurrent I_{PD} to output voltage V_{PD} considering TIA gain G

$$V_{PD} = I_{PD} \cdot G. \quad (6)$$

At the next stage, a receiver or a measurement tool, like a Software Defined Radio (SDR) or a spectrum analyzer is connected. At this step, the PD output voltage V_{PD} can be converted to the power at 50Ω impedance as

$$P_{PD} = \frac{V_{PD}^2}{50\Omega}. \quad (7)$$

Note that, with Equation (1) we can calculate the luminous flux at every point in a 3D space for the range of angles α_h and α_v . This allows us to investigate different PD mounting heights. With Equations (4) to (7) we can calculate a 3D model of the radiometric radiant flux $\Phi_{E,\Omega}$, photocurrent I_{PD} , voltage output V_{PD} , and the power at the next stage P_{PD} , respectively, for any communication distance. If these equations are evaluated on different positions on a plane, spatial distributions of the corresponding quantities can be generated. However, the model currently does not account for hardware-dependent nonlinearities. Figure 1b shows the spatial distribution of the power at an impedance of 50Ω for the left low beam of a sedan.

B. Empirical Measurements

To validate our model we performed measurements at HELLA's *Lichtkanal* (light channel) facility in Lippstadt, Germany. The Lichtkanal is designed to provide ideal conditions for the measurement of automotive lighting modules: the indoor setup helps to suppress outdoor optical channel disturbances, such as sunlight and adverse weather conditions; its walls are painted with special dye that absorbs light and minimizes reflections and other wave propagation phenomena. To closely emulate a real two-lane road, the Lichtkanal has an asphalted surface of 145 m length and 11 m width.

For the measurements we used a pair of modern LED-based headlight modules, which were installed at the beginning of the road. Figure 2 shows the top view of the planned measurement points in the Lichtkanal. The midpoint between the headlights (marked with X) was chosen as the reference point for our measurements. Both headlights were placed at 75 cm on the sides of the reference point, and mounted at 65 cm height.

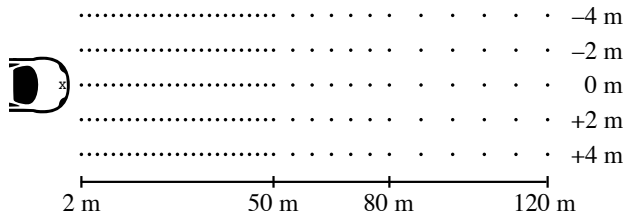


Figure 2. Layout of the measurement points at HELLA's Lichtkanal. Values on the horizontal axis show the distance from the reference point X. The point density indicates the distance between consecutive measurement points.

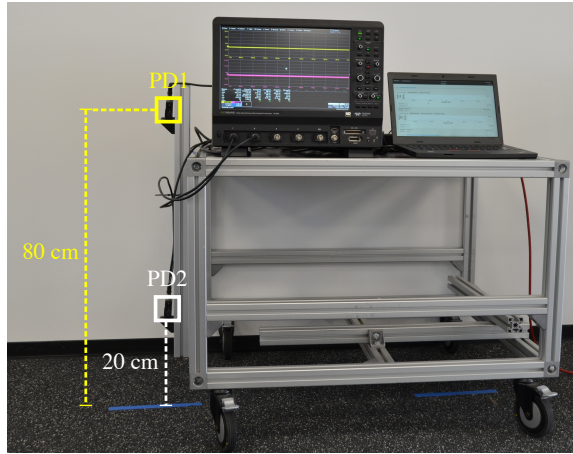


Figure 3. Measurement setup with two Thorlabs PDA100A PDs mounted at different heights, the oscilloscope and the measurement laptop.

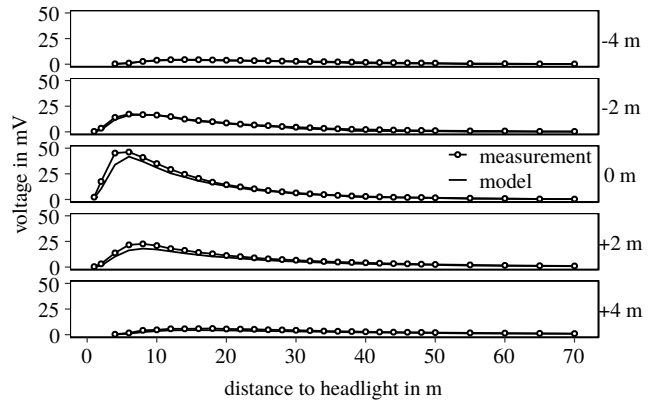
On the receiving end, we used two Thorlabs PDA100A PDs connected to an oscilloscope, to simultaneously measure the voltage at two different heights. One of the PDs was mounted at 20 cm and the other at 80 cm above ground, resembling the height of a license plate² and that of the taillights,³ respectively. Figure 3 shows a side view image of the measurement setup.

To conduct the measurements, we divided the road into three grids with different resolutions for the measurement points (cf. Figure 2). For distances up to 50 m, we performed measurements in steps of 2 m. We reduced the resolution of our measurements for distances beyond 50 m, since the inverse square law applies to light and the difference in measured voltage becomes smaller with growing distance. For the range between 50–80 m, the distance between two points was set to 5 m, while for the distances up to 120 m a measurement was taken every 10 m. All measurements were performed along five parallel lines. The reference line, labeled as 0 m in Figure 2, was aligned with the reference point; the other four lines were distributed equally on each side of the reference line at distances of 2 m and 4 m in both directions.

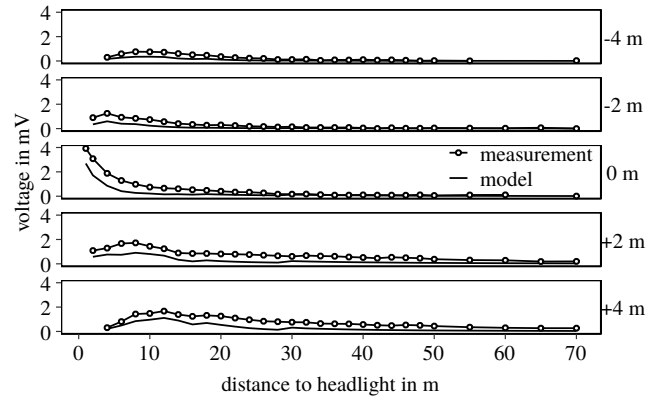
First, we measured the low beam, covering most of the 120 m × 8 m measurement area. Due to technical reasons, we were not able to perform measurements on the farthest points, i.e., beyond 70 m, on the 0 m, 2 m and 4 m lines.

²The lowest legal license plate mounting height in Europe is 20 cm.

³The typical height for taillights in passenger vehicles is 80 cm.



(a) PD at 20 cm height



(b) PD at 80 cm height

Figure 4. Measured voltage and estimated voltage for different PD heights. Measurement data beyond 70 m is partially available, hence we only show data points up to 70 m.

However, due to the inverse square law, this did not have any significant impact on our results, as we will describe later. Also, for practical reasons, for the high beam we conducted measurements only across the reference line, because the high beam has a symmetric radiation pattern and no particular effects were anticipated on the lateral measurement lines.

Figure 4 shows the measured voltage at 20 cm and 80 cm height for the low beam and the estimated voltage from our model, respectively. For each PD, we use a grid of stacked subplots corresponding to the five measurement lines. The horizontal axis is the same for all of the plots, and it shows the distance from the measured headlights to a particular measurement point. Note that Figures 4a and 4b use different vertical axis, because the voltages measured at 80 cm height are much lower compared to the ones measured at 20 cm.

As expected, for the most part the measured voltage is inversely proportional to the distance between the headlights and the PDs. However, it does not decrease equally on each side of the reference line. Higher voltages are measured when a PD is located on the right of the reference line (the +2 m line), as opposed to the left side (the -2 m line). This is due to the asymmetric radiation pattern of the low beam, which is meant to illuminate the road ahead without glaring oncoming traffic in the opposite direction [10], [18].

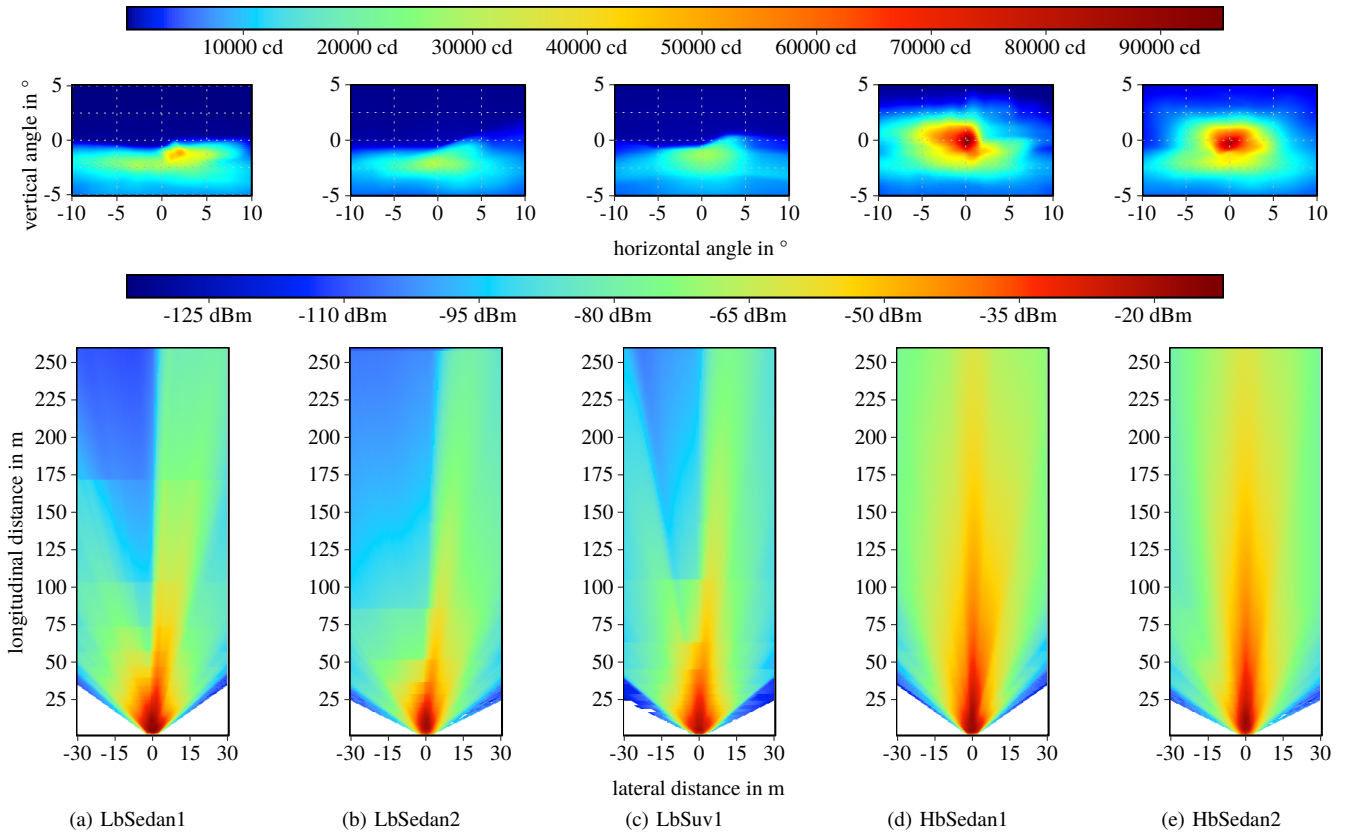


Figure 5. Isocandela plot (of the right lighting module) and corresponding radiation pattern (of both modules) for the considered headlights. Isocandela plots show the luminous intensity (obtained from goniometric measurements), whereas the radiation patterns the received electrical power for a PD at 20 cm height.

Figure 4a shows the measured voltage and the estimated voltage at 20 cm height. The measured voltage is low at short distances. This is due to the height difference between the headlights and the PD, namely, the resulting vertical emission angle. The voltage reaches peak value at 6–14 m distances for all lines, and eventually decays with increasing distance. This rise and fall characteristics strongly differ with lateral displacement due to the increasing horizontal angle of emission. The rise is steeper on the reference line, with a maximum of 48.71 mV at 6 m, and shallower on the ± 2 m and ± 4 m lines. We measured maxima of 6.98 mV at 14 m for the -4 m line, 19.79 mV at 6 m for the -2 m line, 25.1 mV at 8 m for the 2 m line, and 8.53 mV at 14 m for the 4 m line.

Figure 4b shows the measured voltage and the estimated voltage at 80 cm height. The trends are similar to the ones in Figure 4a. However, since the low beams illuminate downwards, and the PD is now located above headlights' horizontal plane, the measured voltage is significantly lower. It is worth noting that for the reference line the maximum voltage of 6.06 mV is already reached at 1 m distance. We further measured maxima of 2.9 mV, 3.39 mV, 3.86 mV, 3.81 mV on the -4 m, -2 m, $+2$ m and $+4$ m lines, respectively.

Based on the presented measurement data, we see that if the low beams are used, a PD mounted at lower height captures more light, thus, would be better suited for communication.

The solid lines in Figures 4a and 4b show the voltage estimated by the model in Section III-A. Our model underestimates

the voltage compared to the measured values, in particular for the PD at 80 cm. This is because we do not account for the NLOS component of the emitted light. Apparently, the accuracy of the model depends on the considered PD position. To characterize the accuracy of the model, we calculated Root-Mean Squared Error (RMSE) of 1.7 mV and 0.39 mV for 20 cm and 80 cm PD height, respectively.

IV. IMPACT OF VEHICLE TYPE AND LIGHTING MODULE

In the following we study five different pairs of headlight modules from three different vehicles: We have the low and the high beam modules of two sedan vehicles and the low beams of one SUV. We identify the light modules based on their type and the corresponding vehicle type and id. For example, the high beam of Sedan 1 is referred to as HbSedan1, whereas the low beam of the SUV 1 as LbSuv1.

A. Light Intensity and Radiation Pattern

Figure 5 shows the isocandela plots and the top-view radiation patterns of the headlights used in our simulations. The isocandela plots, shown in the upper row, are obtained from goniometric measurements. They show the luminous intensity of the emitted light on the vertical plane. The range of horizontal and vertical emission angles is shown in the respective axes. Note that, due to space constraints, we only plot the isocandela plot of the right headlights. Also, these results are sufficient for explaining the relevant effects. To

ensure comparability between low beams and high beams, we use a square root scale for the isocandela plots.

The top-view radiation patterns, plotted in the lower row in Figure 5, are obtained upon applying our model from Section III-A to the goniometric measurements. They plot the electrical power received from the left and the right headlight for a fixed PD height of 20 cm. To account for the height difference between different vehicle types, the radiation patterns of the sedans are plotted for a mounting height of 65 cm, whereas SUV's at 75 cm. The horizontal and vertical axes show the lateral and longitudinal distance to the midpoint between the left and right lighting modules, respectively.

The primary purpose of the low beams is to properly illuminate the road in front of the vehicle, while not glaring the oncoming traffic from the opposite direction. As a result, the low beams are designed to have asymmetric patterns with more power concentrated on the low beam mounted on the same side as the rule of the road in a given country. This asymmetry can be observed in Figures 5a to 5c: all three isocandela plots share the same angle-dependent characteristic. More luminous intensity is concentrated in vertical angles smaller than 0° , with a strong tendency towards positive horizontal angles, i.e., the lower right quadrant of the isocandela plots. LbSedan1 has the highest luminous intensity of almost 50 000 cd at approximately -2° and $+2^\circ$ vertical and horizontal angle, respectively. Whereas, the peaks of the other low beams are closer to the $(0^\circ, 0^\circ)$ origin. Note that, although Sedan 1 and Sedan 2 belong to the same vehicle type their patterns differs vastly.

Compared to the sedans, the SUV has a more evenly distributed luminous intensity, in particular between -5° and $+5^\circ$ horizontal angles. Despite the similarities in their isocandela plots, LbSuv1 and LbSedan2 have very different radiation patterns. In particular, the SUV exhibits higher light intensity characteristics for the range between 50–100 m, where the sedans decay. However, for short distances, it has less power concentrated towards the middle of the radiation pattern. These effects can be explained with the height difference between the two vehicle types.

For the lateral distances, LbSedan2 performs the worst, while LbSedan1 and LbSuv1 have similar radiation characteristics, although their isocandela plots differ.

High beams are meant to illuminate the road at distances greater than the low beam. As a result, they have a stronger and more focused emission of light. The isocandela plots of the high beams show that most of the light is focused around the $(0^\circ, 0^\circ)$ origin. Compared to the low beams, there is significantly more light above the 0° vertical angle, but less for the vertical angles smaller than -3° . This might have nontrivial effects for communication at short distances, if the receiving PD is below the vertical plane of the transmitting high beams.

The high beam of Sedan1 has a maximum luminous intensity of approximately 100 000 cd – double the maximum luminous intensity of its low beam module, which is the brightest among all low beams. Additionally, the high beams have notably less asymmetric patterns, this can be observed best from their radiation patterns. Note that although the high beams of Sedan

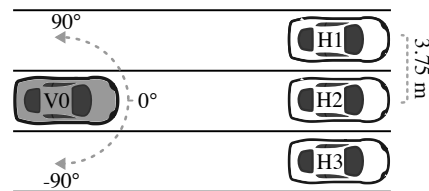


Figure 6. Simulated scenario of a three-lane road. Only the reference vehicle V0 transmits via V-VLC; the other vehicles receive. The distance and angle between V0 and the other vehicles is varied between different simulation runs.

1 and Sedan 2 belong to the same vehicle type, their isocandela plots look significantly different. One reason for this might be the implementation technique of the high beam: HbSedan1 is a standalone high beam module within the headlights of the vehicle, whereas HbSedan2 is implemented by turning on extra LEDs in addition to the ones of the corresponding low beam, (i.e., LbSedan2). That is why the isocandela plot of LbSedan2 and HbSedan2 have similar angle-dependent characteristics, in particular for lower part of the isocandela plot, i.e., vertical angles below -2° . On the other hand, the low beam and the high beam of Sedan 1 have very different isocandela plots.

Naturally, due the higher luminous intensity and more focused light at higher vertical angles, the radiation patterns of the high beams span to larger longitudinal distances compared to the low beams, thus, they present a better candidate for long-distance communication.

B. Vehicular Visible Light Communication Comparison

We implement the model presented in Section III-A in our simulation setup, and integrate all of the previously discussed radiation patterns to Veins VLC [18].⁴ By means of extensive simulations, we investigate the performance and feasibility of these lighting modules for V-VLC. Figure 6 shows the simulated scenario. Here, we model a three-lane road with a reference vehicle in the middle lane and three vehicles in front of the reference vehicle, each on its own lane. The reference vehicle transmits 1023 byte messages via its headlights; the other vehicles receive with the back-mounted PD. The packet size is set to the maximum packet size according to PHY 1 specification of IEEE 802.15.7 for outdoor VLC.

We performed simulations for all five lighting modules presented previously. Depending on the vehicle type, we vary the mounting height of the headlights: 75 cm for the SUV and 65 cm for the sedans. For the receiving vehicles, the PD in the rear is mounted at 20 cm. The lateral distance between two lighting modules in a vehicle is set to 1.5 m. To capture the effects of driving behavior on roads, we rotate the reference vehicle from -90° to 90° in increments of 10° . We also vary the distance between the reference vehicle and the other vehicles in increments of 10 m. For statistical significance the simulations are repeated 10 times for each variation in angle or distance. Table I summarizes the most relevant simulation parameters. The VLC sensitivity threshold is set to an SNR of 0 dB. Whereas, the noise was measured in darkness with the Thorlabs

⁴<http://ccs-labs.org/software/>

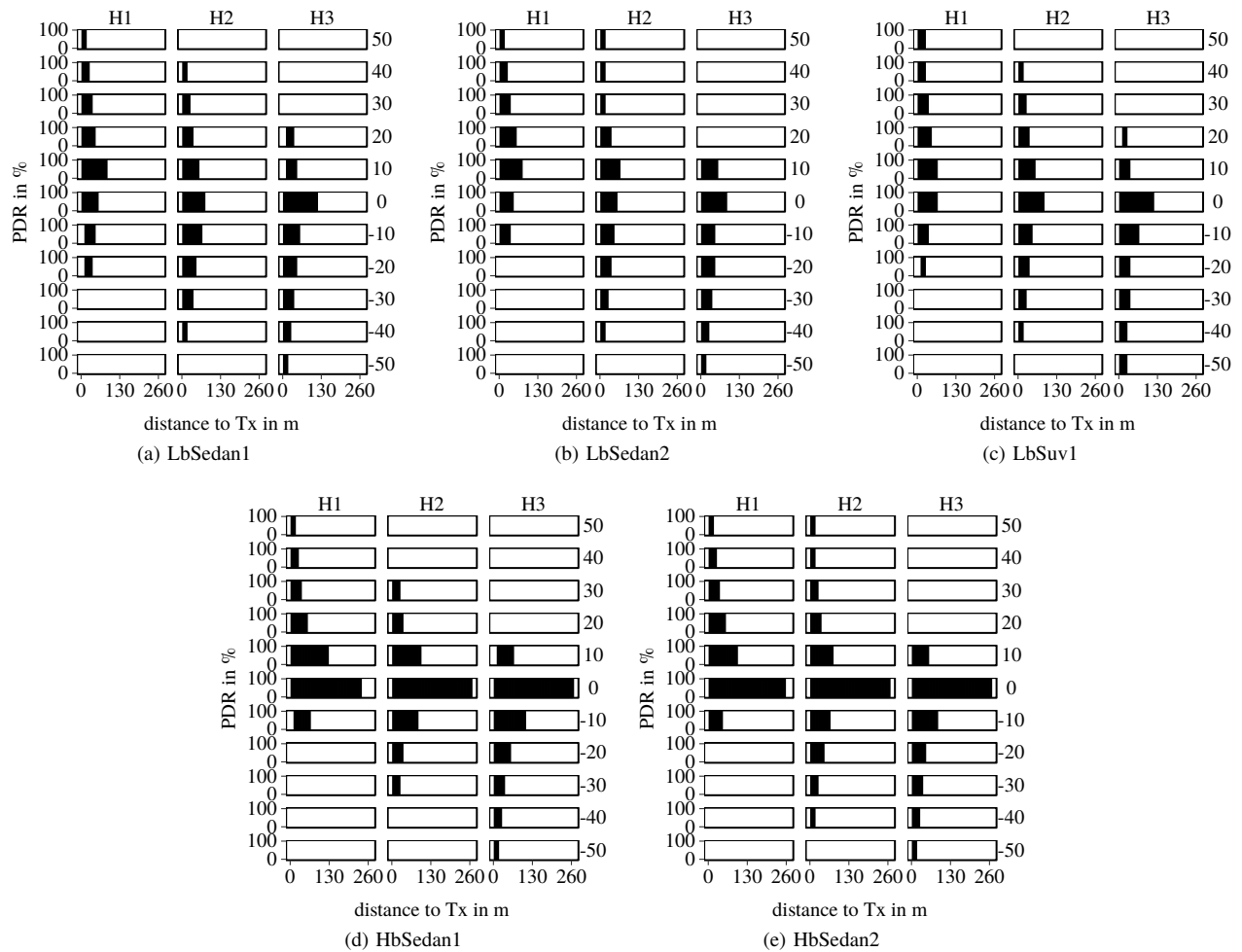


Figure 7. PDR obtained in simulation for all vehicle types and lighting modules.

PDA100A PD and a Le Croy HDO9404-MS oscilloscope for the intensity modulation band between 500 kHz and 2 MHz. Note that noise includes shot, thermal, and quantization noise.

Figure 7 shows the PDR for the packets transmitted at different distances and angles (showing values between -50 – 50°) by the reference vehicle V0. For each low and high beam we have a grid of subplots, where each column represents the PDR plots for one of the receiving vehicles, whereas the rows represent V0's angle of rotation. The distance between V0 and other vehicles is given along the horizontal axis.

Figures 7a to 7c show the PDR for the low beams. As we saw from the isocandela plots and the radiation patterns in Figure 5, the low beams share some common characteristics. This can also be observed in their communication performance.

Table I
SIMULATION PARAMETERS.

Packet length	1023 byte
Modulation and BER model	OOK (as in [18])
VLC sensitivity threshold	-64.75 dBm
Thermal noise	-110 dBm
Headlight height	65 cm or 75 cm
Rear PD height	20 cm

For example, when the reference vehicle is oriented at 0° , thus, pointing in the same direction as the other vehicles, we observe the effects of asymmetric light distribution. The communication link with the vehicle on the right lane, i.e., H3, is better compared to the other vehicles, regardless of the low beam type. Interestingly, even though according to the isocandela plots LbSuv1 has lower luminous intensity than LbSedan1, communication with LbSuv1 is possible for greater distances. In particular, LbSuv1 can communicate up to 120 m with H3, whereas LbSedan1 up to 110 m. We argue that the advantage of LbSuv1 in communication range is a result of SUV's radiation pattern and the higher mounting height of its headlights. LbSedan2 has the lowest communication range of 90 m, however, it has the broadest angular range. This is observed best if we consider the communication with H2: LbSedan1 and LbSuv1 can communicate with H2 for angles of orientation between -40 – 40° , while LbSedan2 can communicate for the range between -50 – 50° .

Another characteristic that is common for all of the headlight modules is that as V0 is rotated to a certain direction, the communication with the vehicle on the opposite direction decreases. $\pm 20^\circ$ appears to be the limit beyond which communication with the vehicle on the opposite direction is

not possible anymore. Communication with such a vehicle is not possible at very short distances because of the directional nature of the light and the shape of the radiation patterns.

Figures 7d and 7e show the PDR for HbSedan1 and HbSedan2, respectively. As expected, because of the much higher luminous intensity, using the high beams for communication provides more than double the communication range of the low beams. With the high beams, V0 can communicate beyond 250 m, given that it is aligned with the vehicle in front of it. Because of the more symmetric and centered emission of the high beams, the increase in communication range only affects angles of rotation between -10° – 10° , where the maximum communication range is reached at 0° rotation angle of V0. This was not the case for the low beams.

We also see the effect of different high beam implementations on the communication performance. Since HbSedan2 is implemented as a superposition of the LbSedan2 and additional LEDs, HbSedan2 inherits the angular characteristics of LbSedan2 for the larger angles of rotation. On the other hand, HbSedan1 and LbSedan1 have very different characteristics. While, HbSedan1 provides a better communication range for the 0° and $\pm 10^{\circ}$ angles, its angular range is smaller than that of LbSedan1. HbSedan2 cannot communicate with H1 and H3 if rotated beyond -10° and 10° , whereas LbSedan2 can maintain this communication for additional 10° in each direction. However, up to the $\pm 10^{\circ}$ angles, HbSedan2 can communicate to farther distances.

The results indicate that an adaptive system might be used for choosing the most appropriate module for communicating with vehicles in a certain direction and distance.

V. CONCLUSION

In this paper, we presented a methodology to investigate the spatial dependency of the performance for Vehicular VLC (V-VLC). Our methodology is able to flexibly cover different lighting modules and receiver mounting heights. Measurements validated our approach to combine given measurement data and analytical calculations. Especially, the integration into the vehicular network simulation framework, Veins, offers a variety of new investigations. With this integration it will be possible to investigate dynamic V-VLC scenarios like platooning, the impact of V-VLC on large scale vehicular networking scenarios and the performance of heterogeneous communication. Most importantly, we were able to use the model to show, for the first time, the impact of vehicle type and headlight module on V-VLC performance; we show that varying factors in lighting module design can have practical impact on potential applications. Our results indicated that future large scale simulation studies should account for the different characteristics of the lighting modules, even if they belong to the same vehicle type.

In future work, we plan to extend our study to taillights and study the impact of different taillight modules on V-VLC. Moreover, we plan to improve the accuracy of our model by integrating the Non Line Of Sight (NLOS) component to it.

VI. ACKNOWLEDGEMENT

The authors would like to thank HELLA GmbH & Co. KGaA for providing access to their facilities and supporting this work. We also thank Samuel Peter Claudel and Qiaoshuang Zhang for their support during the measurement campaign.

REFERENCES

- [1] "Traffic Safety Basic Facts on Main Figures," European Commission, Directorate General for Transport, Tech. Rep., Jun. 2017.
- [2] "A European strategy on Cooperative Intelligent Transport Systems, a milestone towards cooperative, connected and automated mobility," European Commission, Tech. Rep., Nov. 2016.
- [3] F. Dressler, H. Hartenstein, O. Altintas, and O. K. Tonguz, "Inter-Vehicle Communication – Quo Vadis," *IEEE Communications Magazine*, vol. 52, no. 6, pp. 170–177, Jun. 2014.
- [4] S.-H. Yu, O. Shih, H.-M. Tsai, N. Wisitpongphan, and R. Roberts, "Smart automotive lighting for vehicle safety," *IEEE Communications Magazine*, vol. 51, no. 12, pp. 50–59, Dec. 2013.
- [5] C. B. Liu, B. Sadeghi, and E. W. Knightly, "Enabling Vehicular Visible Light Communication (V2LC) Networks," in *ACM VANET 2011*, Las Vegas, NV: ACM, Sep. 2011, 41–50.
- [6] A.-M. Cailean and M. Dimian, "Impact of IEEE 802.15.7 Standard on Visible Light Communications Usage in Automotive Applications," *IEEE Communications Magazine*, 2017.
- [7] "Photobiological Safety of Lamps and Lamp Systems," IEC, Tech. Rep. IEC 62471:2009, Sep. 2009.
- [8] "Uniform Provisions Concerning the Approval of Motor Vehicle Headlamps Emitting an Asymmetrical Passing Beam or a Driving Beam or Both and Equipped with Filament Lamps," United Nations, Tech. Rep. Regulation No. 112 - Revision 1, Oct. 2006.
- [9] C. Sommer, R. German, and F. Dressler, "Bidirectionally Coupled Network and Road Traffic Simulation for Improved IVC Analysis," *IEEE Transactions on Mobile Computing*, vol. 10, no. 1, pp. 3–15, Jan. 2011.
- [10] H.-Y. Tseng, Y.-L. Wei, A.-L. Chen, H.-P. Wu, H. Hsu, and H.-M. Tsai, "Characterizing link asymmetry in vehicle-to-vehicle Visible Light Communications," in *IEEE VNC 2015*, Kyoto, Japan: IEEE, Dec. 2015, pp. 88–95.
- [11] S. Kruse, C. Kress, A. Memedi, C. Tebruegge, M. S. Amjad, C. Scheytt, and F. Dressler, "Design of an Automotive Visible Light Communications Link using an Off-The-Shelf LED Headlight," in *ANALOG 2018*, Munich, Germany: VDE, Sep. 2018.
- [12] O. Narmanlioglu, B. Turan, S. Coleri Ergen, and M. Uysal, "Cooperative MIMO-OFDM based inter-vehicular visible light communication using brake lights," *Elsevier Computer Communications*, vol. 120, no. C, pp. 138–146, May 2018.
- [13] B. Turan, S. Ucar, S. Coleri Ergen, and O. Ozkasap, "Dual Channel Visible Light Communications for Enhanced Vehicular Connectivity," in *IEEE VNC 2015*, Kyoto, Japan: IEEE, Dec. 2015, pp. 84–87.
- [14] D. Eckhoff, A. Brummer, and C. Sommer, "On the Impact of Antenna Patterns on VANET Simulation," in *IEEE VNC 2016*, Columbus, OH: IEEE, Dec. 2016, pp. 17–20.
- [15] B. Tomas, H.-M. Tsai, and M. Boban, "Simulating Vehicular Visible Light Communication: Physical Radio and MAC Modeling," in *IEEE VNC 2014*, Paderborn, Germany: IEEE, Dec. 2014, pp. 222–225.
- [16] W. Viriyasitavat, S.-H. Yu, and H.-M. Tsai, "Channel Model for Visible Light Communications Using Off-the-shelf Scooter Taillight," in *IEEE VNC 2013*, Boston, MA: IEEE, Dec. 2013, pp. 170–173.
- [17] P. Luo, Z. Ghassemlooy, H. Le Minh, E. Bentley, A. Burton, and X. Tang, "Performance analysis of a car-to-car visible light communication system," *Applied Optics*, vol. 54, no. 7, pp. 1696–1706, Mar. 2015.
- [18] A. Memedi, H.-M. Tsai, and F. Dressler, "Impact of Realistic Light Radiation Pattern on Vehicular Visible Light Communication," in *IEEE GLOBECOM 2017*, Singapore: IEEE, Dec. 2017.
- [19] A. Valberg, *Light Vision Color*. John Wiley & Sons, Feb. 2007.
- [20] L. Simonot and P. Boulenguez, "Generalization of the geometric description of a light beam in radiometry and photometry," *Journal of the Optical Society of America A (JOSA A)*, vol. 30, no. 4, 589–595, Apr. 2013.